

**Thermal Analysis on Hex Placement Patterns of the Gemini Primary
Mirrors**

M. K. Cho

Gemini Telescopes Project, 950 N. Cherry Ave., Tucson AZ 85719

W. R. Powell

Corning Incorporated, Science & Technology Division, Corning NY 14831

Gemini Preprint #16

Thermal Analysis on Hex Placement Patterns of the Gemini Primary Mirrors

Myung K. Cho

Optical Sciences Center in the University of Arizona, Tucson, AZ 85721
Gemini Telescopes Project, P.O. Box 26732, Tucson, AZ 85726-6732

William R. Powell

Corning Incorporated, Science & Technology Division
Corning, NY 14831

ABSTRACT

Ultra Low Expansion (ULE)TM material of Corning Glass Work was chosen for the Gemini primary mirrors. The ULE mirror blank becomes monolithic by a fusion process which seals together 55 piece parts from a total of 44 hexagonal segments (hexes). As a consequence of this fusion process, an optical surface distortion due to inhomogeneity in the coefficient of thermal expansion (CTE) is induced. The precise location of the individual hexes in the blank was determined by a detailed analysis in the optimization process. This analysis accommodates two thermal environments, thermal soak of -25°C and thermal gradient of 3°C from the top to bottom surfaces. A parametric design study was conducted to determine an optimized pattern of the hex placements for the Gemini primary mirrors. Active optics corrections were performed to determine the optimum hex patterns. The results indicated that the optical surface distortion due to the CTE deviations was minimized based on the optimized location of the individual hexes. The thermal surface distortion and the optical image quality as well as the plate scale error of the primary mirrors met the design and the scientific requirements. The effect of random errors of the CTE measurement was within the tolerance error budget.

1. INTRODUCTION

The Gemini primary mirrors are made of Corning ULE hex segments to build the 8.1 meter diameter meniscus substrate. The fabrication process requires a total of 55 piece segments from 44 ULE individual hexagonal blanks. Each of the 44 hexes has its own thermal characteristics which are the volumetric average of the radial thermal coefficient (VARC) and the axial CTE gradient. The thermal coefficients of ULE are excellent; however, the variation of CTE and CTE gradients may effect the optical quality.

A mathematical thermal model was employed to quantify the optical surface distortion due to variation of the thermal characteristics. In order to minimize the surface distortion, the CTE distribution of the individual hexes demands an appropriate hex placement. Since the thermal distortion depends solely on the CTE values of hexes and thermal difference, the locations of the hexes mainly govern the optical surface quality. Once the segment placement has been carefully determined, then the segments are fusion sealed together to produce a monolithic mirror blank. Identification numbers of the hex segments of the Gemini primary mirror are shown in Figure 1.

Several design studies were performed to evaluate the optical surface figure errors of large primary mirrors subjected to thermal variations. Cho and Hansen [1] performed a thermal analysis to predict the distortion of the Gemini primary mirror due to temperature gradients (in the radial direction and the axial direction through the thickness), various temperature distribution, and CTE variations within the primary mirror. The optical surface error and its effect on the image quality were described for the cases before and after active optics corrections. Krim et al. [2] performed a preliminary optimization study on ULE hex segment placements. It was reported that the surface error can be significantly improved with a spiral hex arrangement. Sasaki et al. [3] optimized the hex placement pattern of the SUBARU primary mirror based on a merit function used in a neural network.

Two thermal environments were considered in this analysis, thermal soak and thermal gradient. The thermal soak effect considered was to simulate the optical surface distortion caused by a temperature difference of approximately 25°C. In

operation mode, the mirror will be possibly exposed to an environment which may be 25°C cooler than the optic shop where the primary mirror is to be polished and tested. For the thermal gradient effect, analysis was performed for the optical surface distortion caused by a three degree temperature difference through the thickness of the mirror. This is the case when the mirror is exposed instantaneously; therefore, it may experience an extreme temperature difference of 3°C between the top and bottom surfaces.

An objective of this study is to determine an optimized pattern of the hex segment placement. A parametric design study was conducted to minimize the optical surface error due to variation of the thermal characteristics. Optimized hex placement was selected such that the optical surface RMS error is minimum after active optics corrections.

2. FINITE ELEMENT ANALYSIS

Solution for the optical surface distortion in the mirror subjected to thermal variation requires additional term due to the thermal strains. The thermal strains can be characterized in terms of a change in temperature difference and/or a change in thermal expansion coefficient (CTE) value.

The CTE value is an experimentally determined material property, and in general it remains reasonably constant over a moderate thermal excursion. Since the GEMINI mirrors are monolithic by a fusion process, the effects of inhomogeneity in the CTE are to be investigated.

2.1. Description of the Finite Element mirror model

A finite element mirror model with a relatively coarse mesh was employed. The model was used to estimate the optical surface distortion due to the CTE variations in the mirror. Thermal strain distributions over the entire mirror were mathematically modeled and the optical surface distortions were monitored. The coarse finite element mirror model was established using the I-DEAS™ software in order to predict the optical surface deformation caused by the thermal strains. The thermal load was used to simulate the VARC (a) differences and the axial CTE gradient (b) variations. Shown in Figure 2 is a full mirror model used in this analysis. It consists of four layers of solid elements through the thickness of 0.2 meters. The upper layer represents the optical surface and has a spherical radius of curvature of 28.8 meters. The inner and outer diameters are 1.2 and 8.0 meters. The mirror model has a total of 2,580 nodes and 3,720 solid 8-noded solid elements. It was kinematically held by 3 hard supports at the back surface of the mirror.

The material properties of ULE that were used in the finite element mirror model are summarized below.

Coefficient of Thermal Expansion	-40 PPB/°C
CTE Maximum Variation	+/-15 PPB/°C
Density	2.205 gm/cm ³
Poisson's Ratio	0.17
Elastic Modulus	67.6 GPa

2.2. Brief Theoretical background for thermal analysis in Finite Element Analysis

In general thermal analysis by the finite element method [4], the stress-strain relationship in an element is defined as:

$$S_i = D_{ij} (B_{ij} \bar{d}_i^e - \epsilon_j^o) + S_i^o \quad (1)$$

,where S_i is a stress tensor, D_{ij} is the elastic tensor, B_{ij} is the strain tensor, \bar{d}_i^e is the nodal displacement of the element, ϵ_j^o is the initial strain (in this case thermal strain) tensor, and S_i^o is the initial stress tensor. The thermal strain due to temperature variation becomes:

$$\epsilon^o = \alpha DT \quad (2)$$

or due to variation of CTE is:

$$\epsilon^o = \alpha \Delta T \quad (3)$$

, where α is the CTE and T is the nodal temperature in the finite element model. Hence, the resulting nodal force due to thermal strain yields:

$$f_i^t = \int_v (B_{ij} D_{ji} \epsilon_i^o) \kappa \quad (4)$$

, where f_i^t is the nodal force tensor calculated from integration over the volume of the element. From the stiffness equation, $F = K D$, the displacement field of an elastic body, D , can be calculated with respect to the system stiffness, K , and the specific force set, F . In thermal analysis, the force set gives rise to thermal deformations in the body. This deformation is normally in a mode with combinations of 'in-plane mode', 'axial mode', and 'out-of-plane bending mode'.

2.3. Effect of VARC distribution

The VARC deviation of the individual hexes causes a variation of thermal strains along the thickness of the mirror. As a consequence, a high order spatial frequency print-through remains on the optical surface. Since the print-through effect varies between the hexes, the distortion on the optical surface is a superposition of the step functions of the individual hexes. To quantify the stepwise irregularity caused by the differences in the volumetric average CTE between the hexes, a set of thermal strain distributions was considered.

Thermal strain due to CTE difference was defined in Equation (3). To establish a data set for the CTE variations in finite element analysis, it commonly requires to assign the individual material property set to the elements in a hex. In the case of many elements with CTE variations, generally it is not a simple task and requires significant amount of time and efforts to prepare the data set. However, the thermal strain in Equation (2) can be employed which is expressed in terms of temperature difference with a constant CTE. In this approach, the thermal strains are treated by a set of the nodal temperatures. This implementation gives much more flexibility to investigate the thermal effect in this parametric study because the nodal temperatures can be dealt by generic nodal loading terms. The following expression which is a combination of two trigonometric functions was employed for an average temperature loading distribution across the radius of the primary mirror:

$$T_a(r) = A \sin \frac{m\pi r}{2R_o} + B \cos \quad (5)$$

, where $T_a(r)$ is the temperature distribution based on α and is a function of a radial location of r . A and B are constants, R_o is the radius of the primary mirror, and n and m are integers which vary from 0 to 4. This temperature distribution represents an average temperature variation at a given location r . It assumes that the VARC distribution is uniform within the elements in a hex. It implies that the distribution does not include the effect from temperature gradient through the thickness of the mirror, which is the axial temperature gradient. The effect of the axial temperature gradient will be discussed the next section. It further assumes that the distribution is cyclic symmetric. Hence, the thermal strains are independent of azimuthal angle.

A set of thermal strain distributions using the temperature distributions specified in Equation (5) was generated. These distributions were then applied to the finite element mirror model. Since these thermal loading inputs give rise to a bulk change in the individual hexes, the resulting optical surface distortion is characterized as a combined mode of 'in-plane mode' and 'axial mode'. The out-of-plane stresses which cause surface bending of the mirror do not occur with these thermal strains.

The thermal distortions were monitored and a data reduction was performed. Aberrations of piston, tilts, and focus were removed from each of the raw optical surface, and then active optics corrections were performed. Listed in Table 1 were the selected results due to the thermal strains using equation (5) for the average temperature distributions.

Table 1. Optical surface errors due to VARC distributions

Mode ID	P.T.F removed		Active correction		Active force
	P-V (nm)	rms (nm)	P-V (nm)	rms (nm)	Fmax (N)

1	84	23	1.2	0.17	5.1
2	30	9	1.7	0.25	4.2
3	95	27	1.6	0.24	5.3
4	223	63	3.2	0.44	12.8

Mode 1 in Table 1 is for a sine distribution with $m=1$ and Mode 2 is for $m=2$. Mode 3 and 4 are for cosine distributions with $n=1$ and $n=2$, respectively. Mode 1 predicted the best surface figure after active optics correction among these various temperature distributions. This implies that the lowest residual surface RMS error after active optics corrections can be obtained if the distribution of nodal temperatures is in a sine form as:

$$T_a(r) = A \sin \frac{pr}{2R} \quad (6)$$

Hence, the effect of VARC can be minimized if the CTE measurements of the individual hexes are arranged in the same fashion as in the above equation. This holds only true in view of the residual surface errors after performing active optics corrections with the active optics system of GEMINI [5].

On other hand, the lowest surface errors before active optics corrections does not necessarily occur at the same mode. As listed in the Table, the lowest surface RMS error before correction was found at Mode 2. The surface errors of this mode are approximately three times better than those of the optimum one (Mode 1).

2.4. Effect of Axial CTE gradient

The CTE measurements from the top surface to the bottom surface in the individual hexes would not be the same in general. This CTE variation along the thickness of the mirror is defined as axial CTE gradient, b . This axial CTE gradient causes the individual hexes to deform in out-of-plane bending mode - in tension on one surface and in compression on the other.

Consequently, the deviation of b in overall hex segments produces a global surface irregularity as a linear combination of the individual bending modes. In order to simulate the effect of deviation in the CTE gradients to the optical surface distortion, a thermal strain distribution was considered as in the previous section. The strains from the CTE gradients through the thickness of the mirror are implemented as the following temperature distribution:

$$T_b(r, z) = A \frac{z}{h} \sin \frac{mpr}{2R_o} + B \frac{z}{h} \cos \quad (7)$$

,where $T_b(r, z)$ is a temperature distribution whose mean value is equal to zero. It varies linearly with the distance through the thickness, z , and has a combined distribution of sine and cosine functions. A and B are coefficients and h is the thickness of the mirror. Integers m and n in trigonometric functions were assumed to vary from 1 to 8. This equation assumes that the temperature field is in a cyclic symmetric distribution. This temperature distribution will cause the mirror to deform in 'out-of-plane bending mode'. For general CTE gradient cases, however, the surface deformation includes 'in-plane mode' as well. The reason is that in most cases the mean of CTE measurements through the thickness is not equal to zero. Therefore, the deformed shape does not always become asymmetric about the middle plane of the mirror model.

The nodal temperature distributions specified in Equation (7) were generated systematically, and they were applied to the finite element mirror model. In analysis, several additional temperature gradient cases were considered which were distributed in functions of the radial locations. The analysis also included the effects due to the temperature distributions of a uniform, linear variation, asymmetric variation, and combinations with others.

The thermal distortions of the optical surface were calculated. Aberrations of piston, tilts, and focus were removed from the raw optical surface deformation, and then active optics corrections were performed. Listed in Table 2 were the selected results due to the thermal strains based on the temperature gradients.

Table 2. Optical surface errors due to the axial CTE gradients

P.T.F removed	Active correction	Active force
---------------	-------------------	--------------

Mode ID	P-V (nm)	rms (nm)	P-V (nm)	rms (nm)	Fmax (N)
1	91	25	5	0.8	26
2	113	25	7	0.8	8
3	78	13	11	1.1	29
4	73	14	9	0.9	8
5	62	17	8	1.1	28
6	102	28	5	0.8	8
7	90	21	9	1.2	13
8	82	19	10	1.1	12
9	80	21	8	0.9	10

Mode 1 in the Table is for a sine distribution with $m=1$ in Equation (7), Mode 2 is for $m=2$, and Mode 3 is for $m=3$. Mode 4, 5, and 6 are for cosine distributions with $n=1$, $n=2$, and $n=3$, respectively. Mode 7 shows results for a linear radial distribution. Mode 8 and 9 are combined cases. It was found that Mode 2 produced the least surface figure errors after active optics correction among various temperature distributions. In other words, the optimum thermal strain distribution was found when a temperature distribution was in a sine function as:

$$T_b(r, z) = A \frac{z}{h} \sin \frac{\pi}{2} \quad (8)$$

The above equation represents a temperature field with a linear gradient over the thickness, h , at a given radial location r . Hence, the optical surface figure will be optimum if the individual hex placements are arranged so that the CTE measurements are in the same distribution as in above equation. Again this holds true only in view of the residual surface errors after active optics corrections by the active optics system of GEMINI. The lowest surface RMS error, however, before active optics correction was found at Mode 3. The uncorrected surface errors of this mode are approximately twice as good as those of the optimum one (Mode 2).

3. HEX PLACEMENT STRATEGY

Actual CTE measurements of the individual hexes for the GEMINI primary mirror blanks were made at Corning Incorporated. The VARC distribution and the axial CTE gradients were examined and processed to generate a data set for the analysis. The range of axial CTE gradient variation between hexes was ± 7 PPB per degree Celsius, and the volumetric average radial CTE was ± 5 PPB per degree. These CTE measurements were based on actual GEMINI Project boules fabricated and tested.

A fine detailed finite element mirror model was established. The fine mesh model is required to predict the optical surface deformation based on actual measurements of VARC differences and the axial CTE gradient variations. Shown in Figure 3 is a full mirror model used in this analysis. It consists of four layers of solid elements through the thickness, and has a total of 21,100 nodes and 11,200 solid 8-noded solid elements. A total of 176 material property data sets were employed to identify the CTE values of the individual hexes in the mirror model.

A parametric study was conducted to determine optimum placements of the hexes for the GEMINI primary mirrors. Initially, optimization started by placing the hexes in the patterns described in Equations (6) and (8). There existed two options to take into consideration for the initial placement, a placement based on either Equation (6) or (8). Incentive was placed to the pattern in Equation (8) over (6) because thermal strains from CTE gradient variations would produce a global surface distortion. Several trade-off iterations were made to accomplish a minimum optical surface error by swapping around the hex locations. To each iteration, optical data reduction was processed with the optical surface deformation. Residual optical surface errors after active optics corrections were monitored. This iteration continued for every possible hex placement combinations. It was found that the fluctuation of the optical surface quality would not be highly sensitive after active optics corrections during the iterations. The final optical surface quality tended to be influenced mostly by the initial placement. Since a limited number of hexes are available from the mirror fabricator, it is not always possible to fulfill the optimum distribution for the initial placement. In this stage, a parametric analysis, a trade-off study, engineering judgment, and engineering intuition are required.

4. RESULTS

Through several iterations and parametric analyses based on the actual CTE measurements for the GEMINI Project primary mirrors, optimum hex placement patterns were determined. From the statistical data of the CTE measurements, overall axial CTE gradient variations were very similar for the hexes in both primary mirrors. Whereas the volumetric CTE values in the primary mirror blank #2 apparently appeared to have a higher and wider distribution than the blank #1.

Thermal and optical analyses were performed to accommodate the two thermal environments, thermal soak of -25°C and thermal gradient of -3°C through the thickness of the mirror. The evaluation of the optical image quality as well as the plate scale error was made. Additionally, the effect of random errors in the CTE measurement was investigated for the mirror in the optimized hex placement pattern.

4.1. Surface distortions

For the primary mirror blank #1 under a 25°C thermal soak (CASE_1S), a P-V of 1,980 nm and a surface RMS of 580 nm were calculated from the RAW data. The optical surface contour map for this RAW data is shown in Figure 4. A P-V of 430 nm and an RMS of 105 nm were calculated after piston, tilts, and focus were removed. A residual surface RMS error of 9 nm with a maximum active force of 48 N was calculated. The optical surface contour maps of this case both before and after active optics corrections are shown in Figure 5. For a 3°C thermal gradient case with a mean CTE of -40 PPB per degree Celsius (CASE_1G), a surface RMS of 80 nm was calculated after piston, tilts, and focus removed. A residual surface RMS error of 12 nm with a maximum active force of 70 N was calculated. The optical surface contour maps for this blank both before and after active optics corrections are shown in Figure 6.

For the primary mirror blank #2 under a 25°C thermal soak (CASE_2S), a P-V of 1,140 nm and a surface RMS of 250 nm were calculated from the RAW data. A P-V of 676 nm and an RMS of 144 nm were calculated after piston, tilts, and focus removed. A residual surface RMS error of 10 nm with a maximum active force of 55 N was calculated. The optical surface contour maps for the blank #2 both before and after active optics corrections are shown in Figure 7. For a 3°C thermal gradient case with a mean CTE of -40 PPB per degree Celsius (CASE_2G), a surface RMS of 86 nm was calculated after piston, tilts, and focus removed. A residual surface RMS error of 12 nm with a maximum active force of 75 N was calculated. The optical surface contour maps both before and after active optics corrections are shown in Figure 8.

Table 3 summarizes the optical surface RMS errors for the primary mirrors before and after active optics corrections for the two thermal environments. Maximum active optics forces required to correct the surface errors were also listed.

Table 3. Summary of thermal deformations of primary mirrors.

CASE ID	RAW DATA RMS (nm)	P.T.F. removed RMS (nm)	ACTIVE optics correction RMS (nm)	Fmax (N)
CASE_1S	580	105	9	48
CASE_1G	691	80	12	70
CASE_2S	250	144	10	55
CASE_2G	680	86	12	75

4.2. Effect on Image Quality and Plate Scale

The overall image degradation allowance for the thermal deformation of the primary mirror is .005 arcsecond increase in diameter for 50% encircled energy and .009 arcsecond for 85% encircled energy at a wavelength of 2200 nm. Requirements also exist for the change in telescope effective focal length caused by the primary mirror assembly. The total allowable change in plate scale is for primary mirror thermal errors is 45 parts per million (ppm). It is assumed that spherical curvature changes of the primary mirror will not be detected by the active optics wavefront sensor because the auto focus system will continually compensate. Therefore, it is assumed that the plate scale changes will not be corrected by the active optics system.

Encircled energy was calculated using the diffraction based on PSF option of CODE V. The interferogram files with a grid size of 512 by 512 were generated. All image quality calculations were performed for the on axis field position. For CASE_1S, the point spread function (PSF) at a wavelength (wl) of 550 nm was plotted in Figure 9. The same PSF plot with a cutoff frequency of -40 dB is shown in Figure 9. Encircled energy diagram at a wavelength of 2200 nm for this case is shown in Figure 10. For CASE_1G, PSF plot with a cutoff frequency of -40 dB and encircled energy plot are shown in Figures 11. Similarly, for CASE_2S, PSF plot with a cutoff frequency of -40 dB and encircled energy plot are shown in Figures 12. PSF plot with a cutoff frequency of -40 dB and encircled energy plot for CASE_2G are shown in Figures 13.

Plate scale changes were evaluated using the amount of focus aberration removed from the deformations of the finite element analysis. Paraxial ray trace analysis results show a plate scale change of one part in one million for a peak to valley change in focus aberration of the primary mirror of 159.9 nm.

Table 4 summarizes the effects on image quality degradation for all of the deformations after active correction as well as plate scale change. The values shown in the table are the overall image size of 50 and 85 percent encircled energy diameters.

Table 4. Summary of image quality and plate scale.

CASE ID	50% Encircled energy (arcsec)	85% Encircled energy (arcsec)	Plate scale changed (PPM)
CASE_1S	0.064	0.199	11.0
CASE_1G	0.065	0.199	13.8
CASE_2S	0.065	0.198	3.1
CASE_2G	0.065	0.199	13.5

Maximum image degradations calculated were 0.0001 arcsecond increase in diameter for 50% encircled energy and 0.0058 arcsecond increase for 85% encircled energy at a wavelength of 2200 nm. These image quality values and the plate scale changes were within the thermal error allowance.

4.3. Effect of Random errors of CTE measurements

The radial volumetric average CTE and the axial CTE gradients were determined from a statistical process based on actual CTE measurements of the individual hexes for the primary mirror blanks. Effects on the optical surface distortion due to random errors in the CTE measurements were examined. A thermal analysis was performed with several random distributions

in the CTE measurements. The following assumptions were made to the CTE distributions: (1) random Gaussian distribution, (2) VARC varies randomly with a range of +/- 1 PPB per degree Celsius, (3) axial CTE gradients are in +/- 1 PPB per degree.

Table 5 listed the optical surface distortion due to the random CTE distributions for the primary mirrors with optimized hex placements. It summarizes the mean values of the results based on random distributions before and after active optics corrections for the two thermal environments.

Table 5. Summary of the mean of random thermal deformations.

CASE	RAW DATA RMS (nm)	P.T.F. removed RMS (nm)	ACTIVE optics correction RMS (nm)	Fmax (N)
SOAK (-25°C)	25	25	1	10
Gradient (-3°C)	3	3	0.2	2

5. SUMMARY AND CONCLUSIONS

A parametric study was performed to minimize the effect of the optical thermal distortions of the primary mirrors for the GEMINI Telescopes Project. Optimum hex placement patterns were determined based on the minimum optical surface RMS errors after active optics corrections. Finite element analysis was employed to quantify the optical surface thermal distortions for the cases of -25°C thermal soak and 3°C thermal gradient. The evaluation of the optical image quality was performed by CODE V. Several program codes developed by GEMINI staff were used to evaluate the performances and to conduct the data reduction process.

It was found that the results from the thermal analysis for both primary mirrors were excellent. For the thermal soak case, a surface RMS error of approximately 10 nm after active optics corrections was calculated for both mirrors. Maximum active force approximately 50 Newtons was required to correct the optical figure errors. The optical surface distortion of the blank #2 tended to be slightly higher (10%) than that of blank #1. The reason was that the distribution of actual CTE measurements of the blank #2 had a wider band and higher peak values.

Based on the results of this study, the thermal distortion and the optical image quality as well as the plate scale error of the primary mirrors satisfied the requirements. The effect of random errors in the CTE measurements was within the tolerance error budget. The optical surface distortions due to thermal gradient for the optimized hex placement patterns were compared with a parallel thermal analysis conducted by Corning. This independent analysis verified the thermal model and demonstrated that the results were in an excellent agreement with those presented herein.

6. REFERENCES

1. M. K. Cho and E. K. Hansen, "Distortion of the Primary Mirror due to Temperature and CTE Nonuniformity", Gemini Report RTP-O-G0034, Tucson, 1994.
2. M. Krim, G. Ruthven, and B. Skrobacz, "Accommodating CTE Discontinuities in a ULE Mosaic Mirror", SPIE Vol. 1236, Tucson, 1990.
3. A. Sasaki, et al., "Primary Mirror Blank Fabrication of SUBARU Telescope", Advanced Technology Optical Telescope V, SPIE Vol. 2199, Hawaii, 1994.
4. O. C. Zienkiewicz, "The Finite Element Method in Engineering Science", McGraw-Hill, New York, 1971.
5. L. M. Stepp, E. W. Huang, and M. K. Cho, "Gemini Primary Mirror Support System", Advanced Technology Optical Telescope V, SPIE Vol. 2199, Hawaii, 1994.

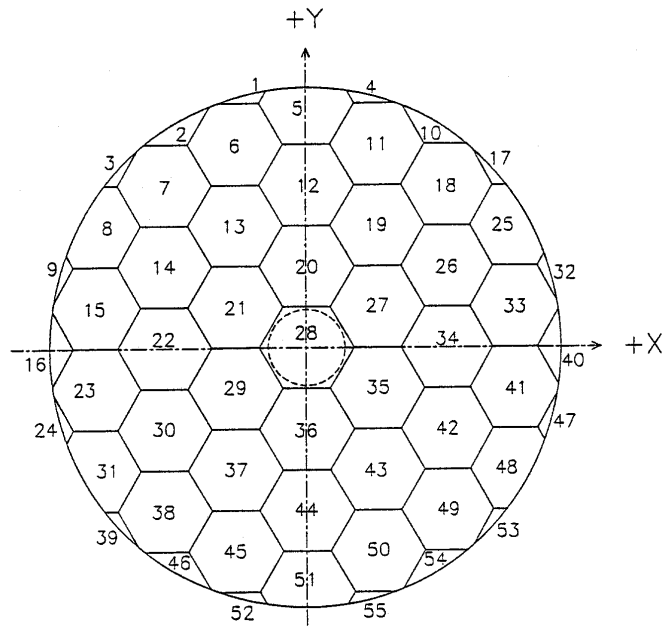


Figure 1. Hex location key for the GEMINI mirror blank.

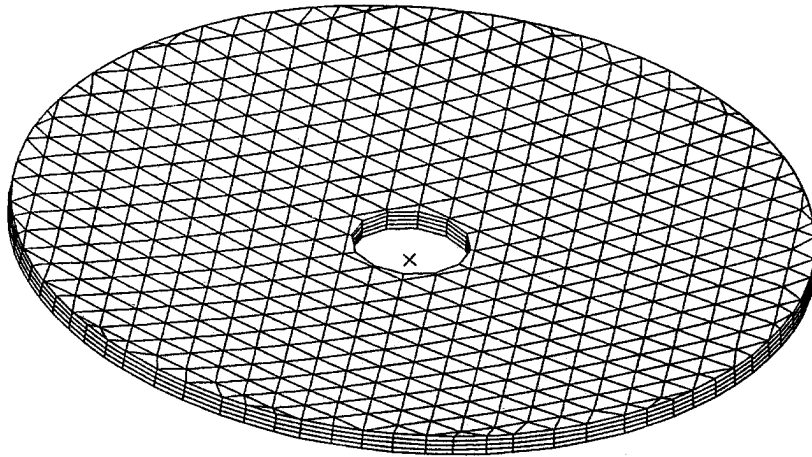


Figure 2. A coarse mesh finite element mirror model used for thermal strain distributions

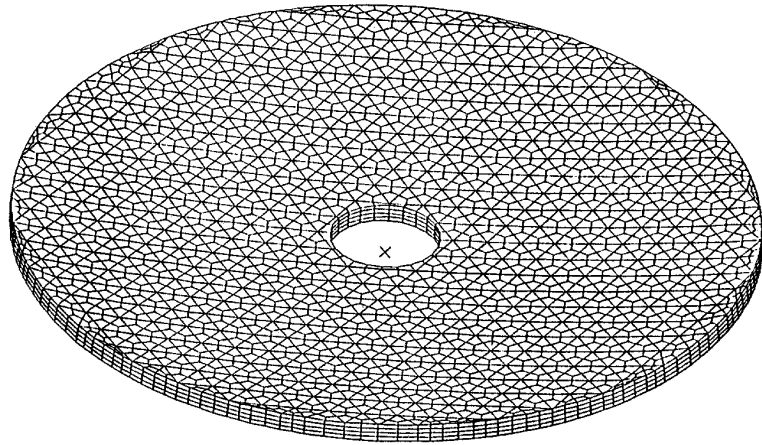


Figure 3. A fine mesh finite element mirror model used for hex placement

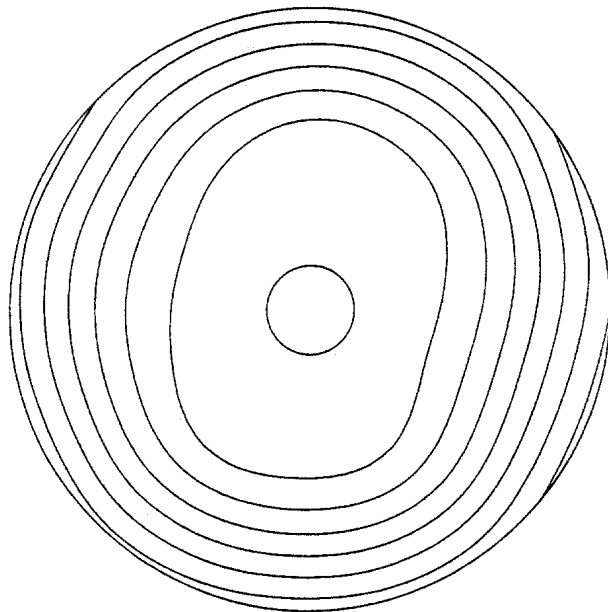


Figure 4. Optical surface contour map for a RAW data (CASE_1S)

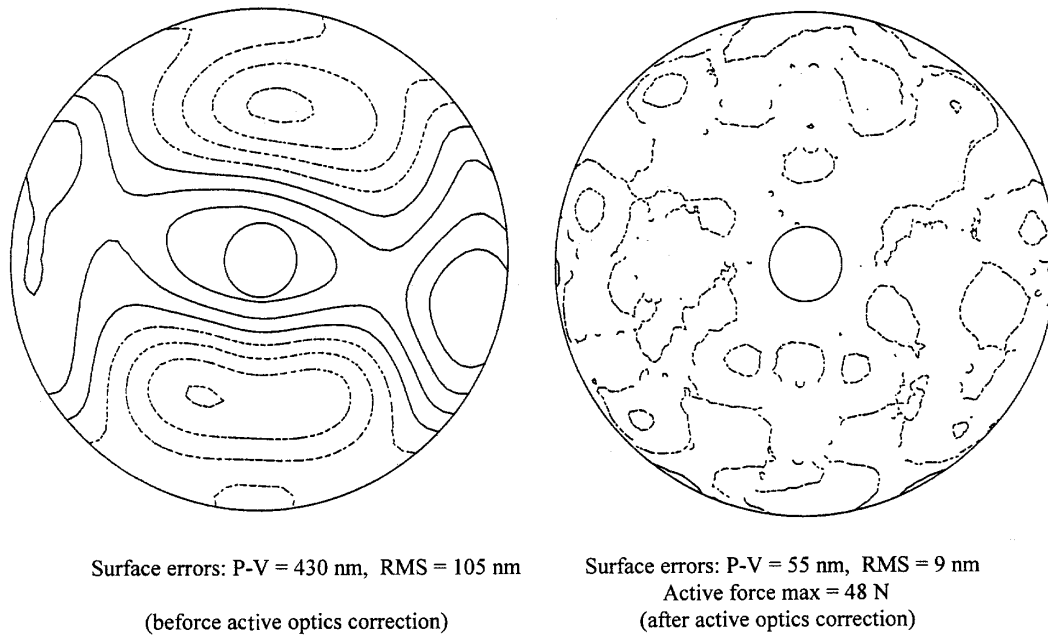


Figure 5. Surface maps before and after active optics correction (CASE_1S)

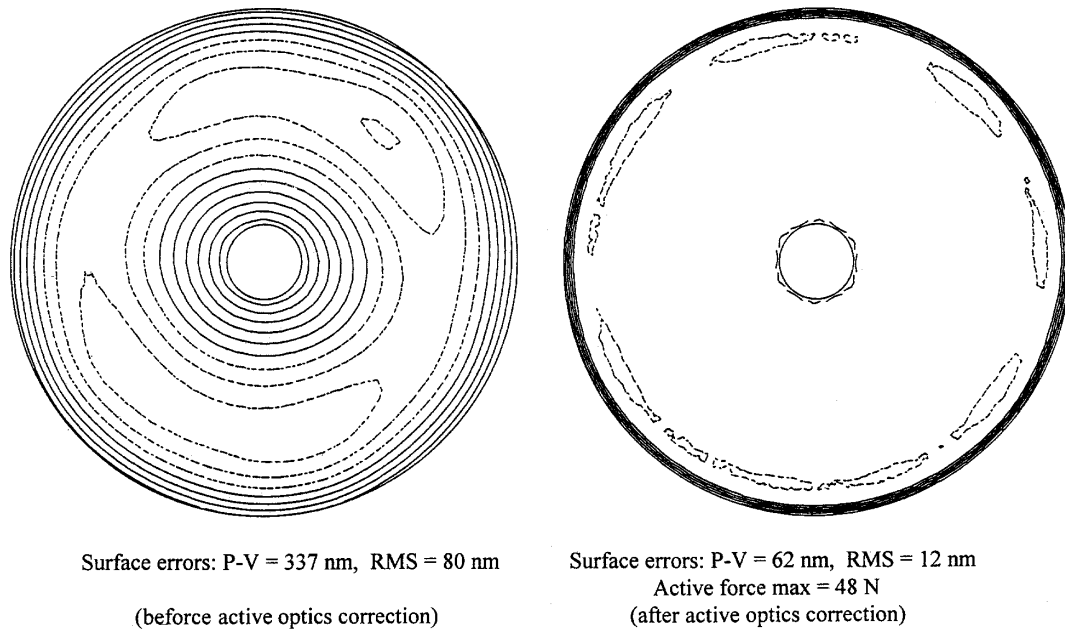


Figure 6. Surface maps before and after active optics correction (CASE_1G)

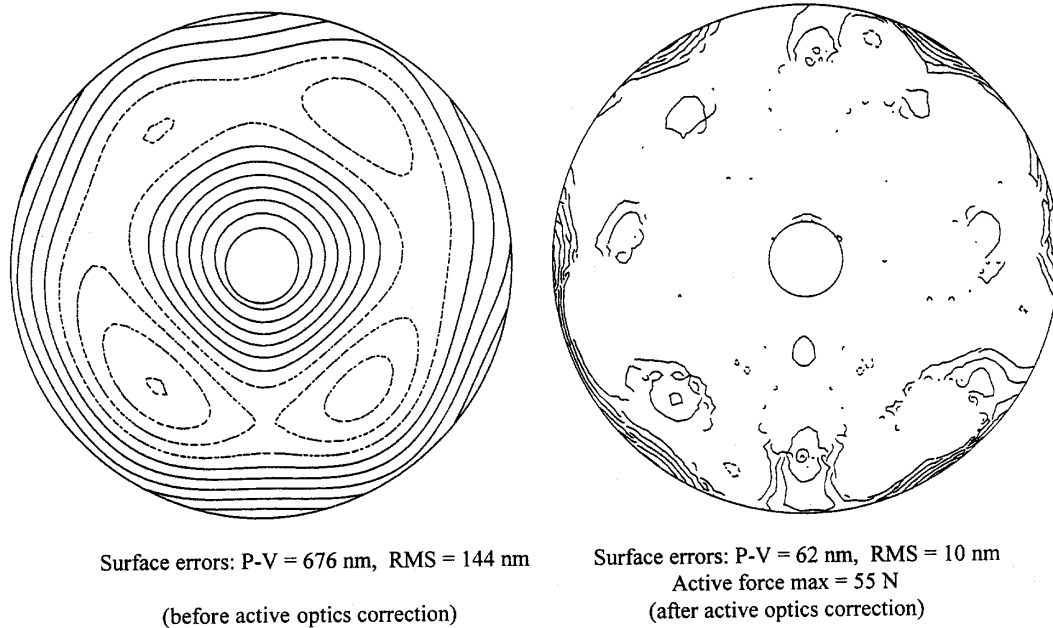


Figure 7. Surface maps before and after active optics correction (CASE_2S)

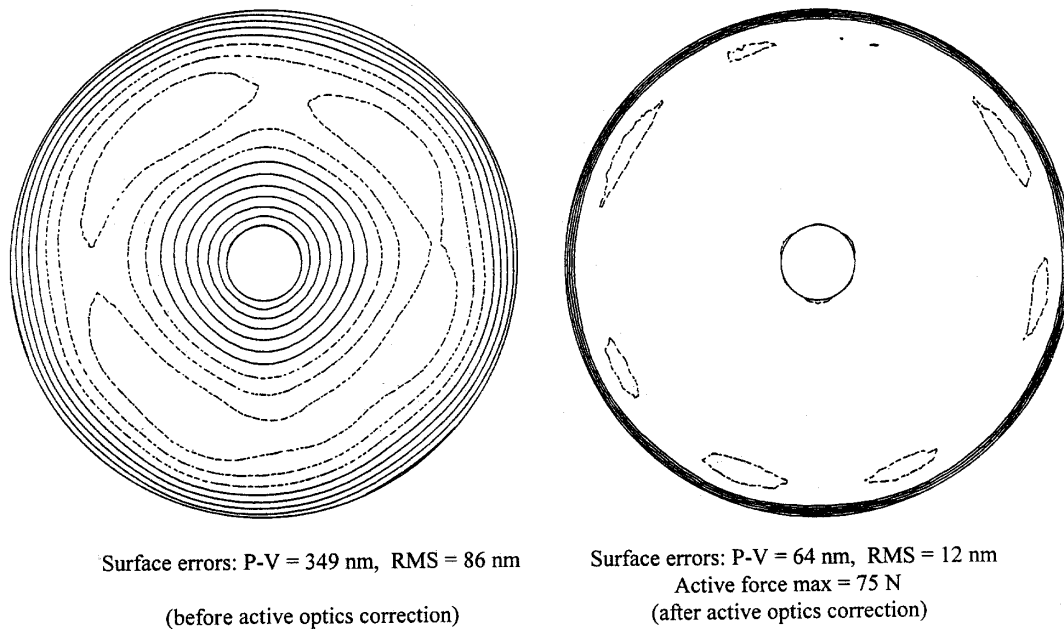


Figure 8. Surface maps before and after active optics correction (CASE_2G)

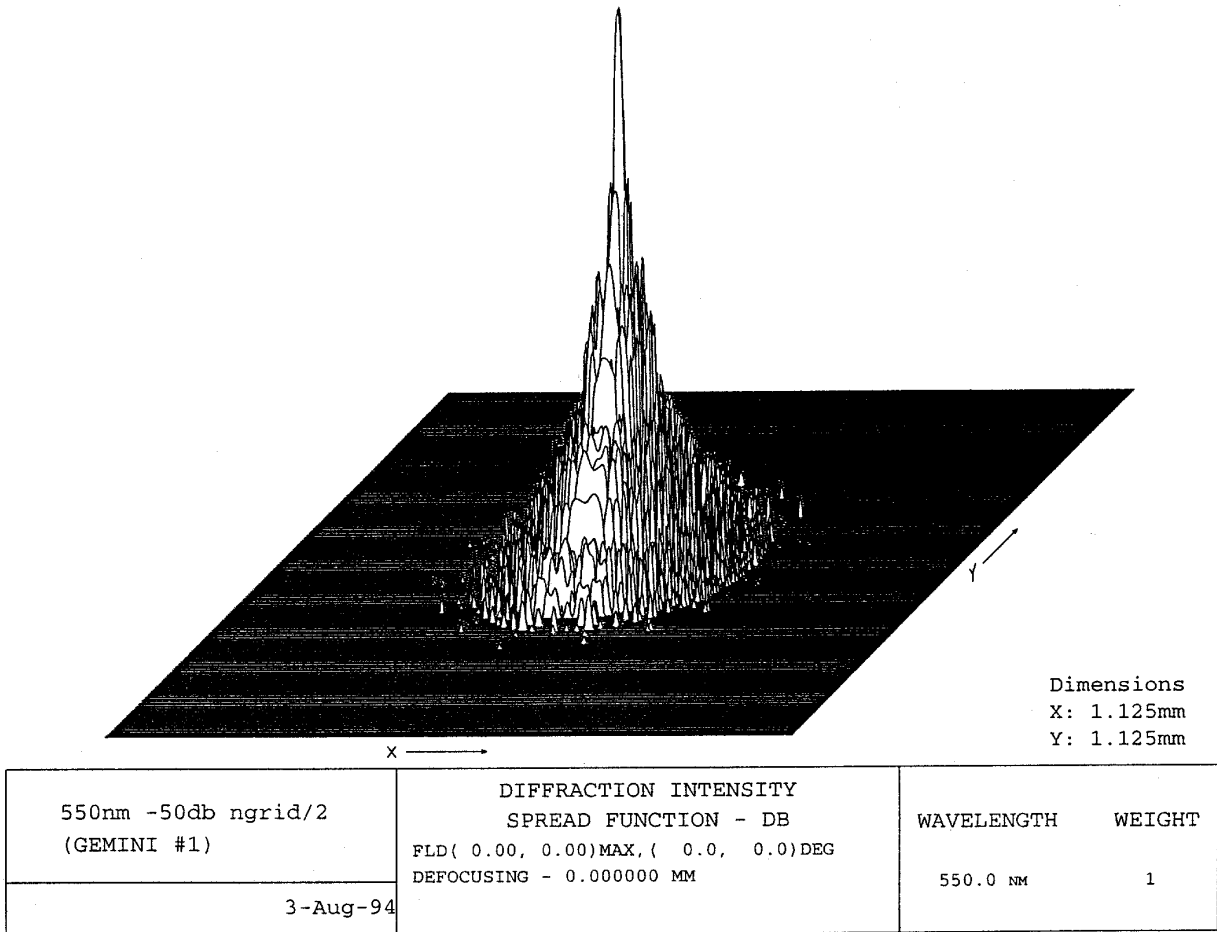
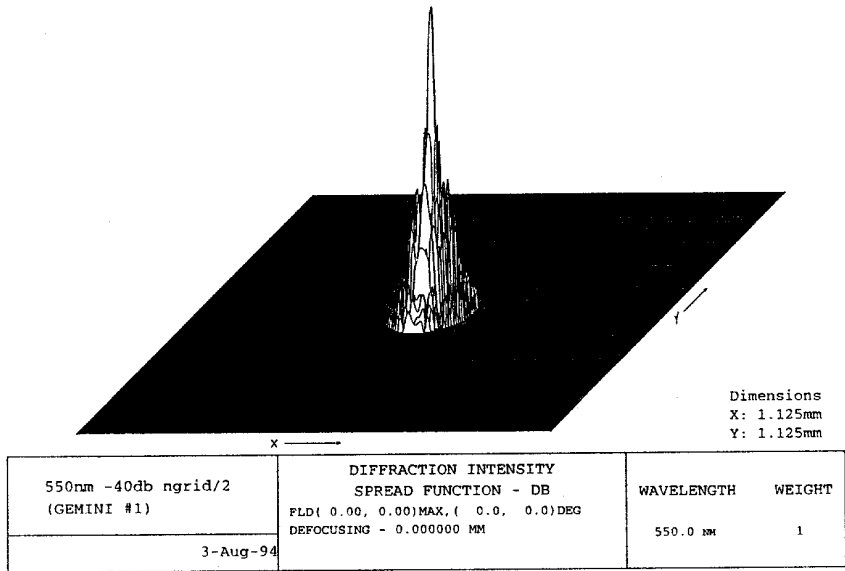
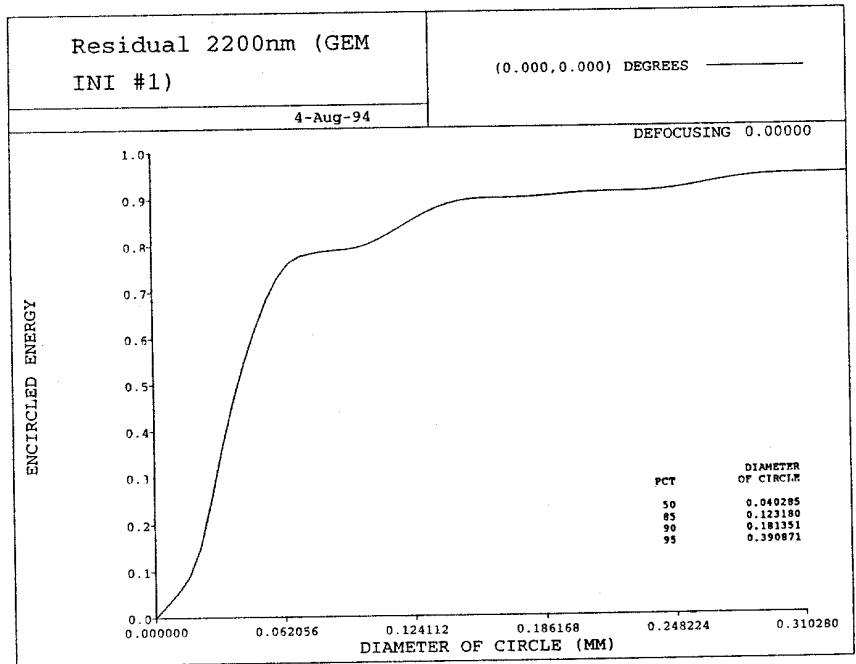


Figure 9. PSF plot with cutoff = -50 dB at wavelength of 550 nm (CASE_1S)

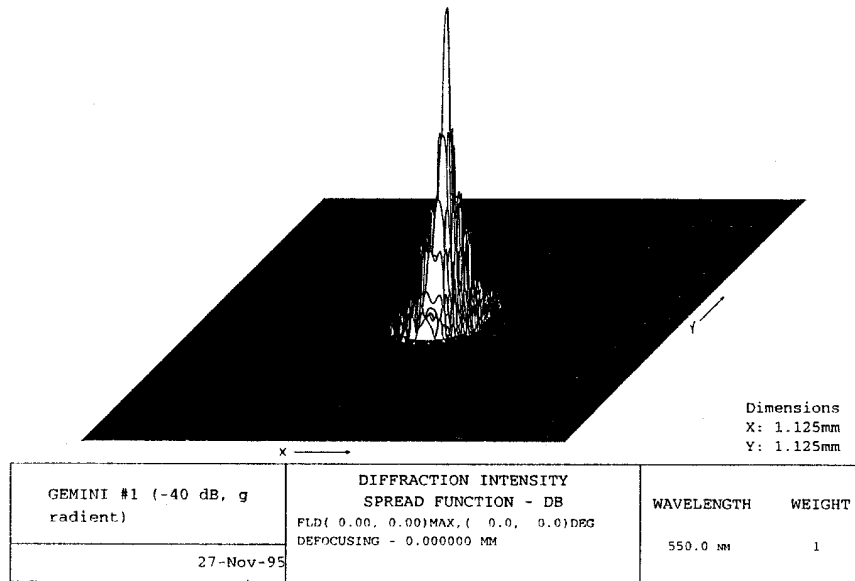


(PSF plot with cutoff = -40 dB at wl = 550 nm)

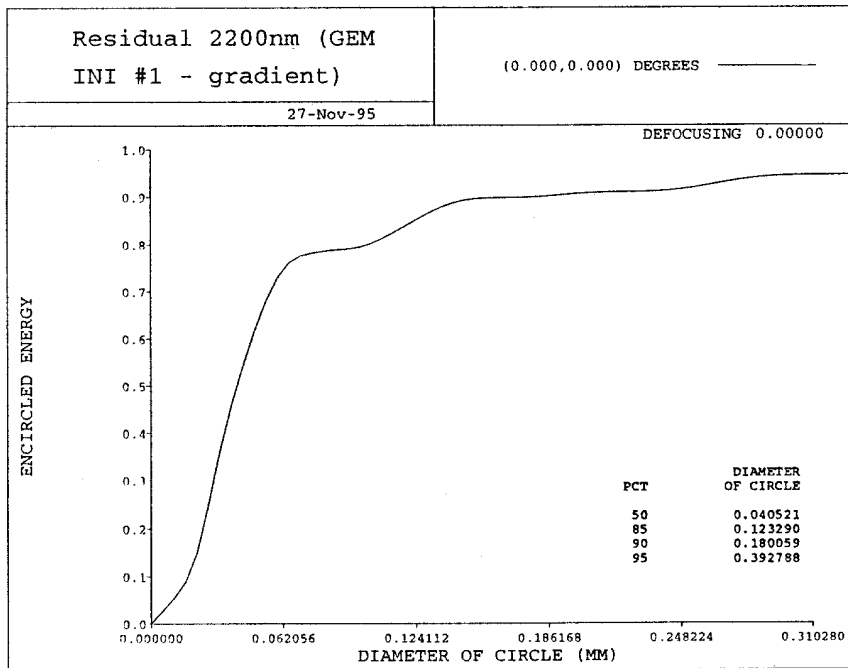


(Encircled energy plot at wl = 2200 nm)

Figure 10. PSF and Encircled energy plots (CASE_1S)

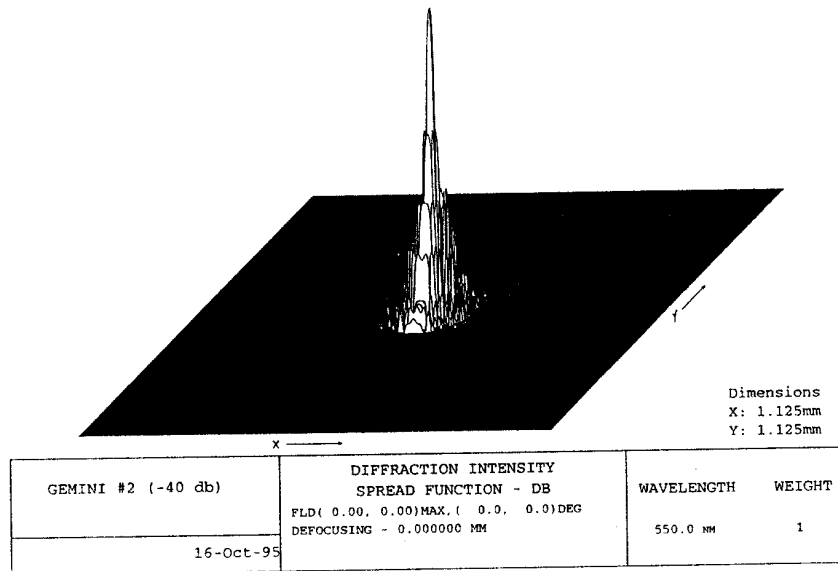


(PSF plot with cutoff = -40 dB at wl = 550 nm)

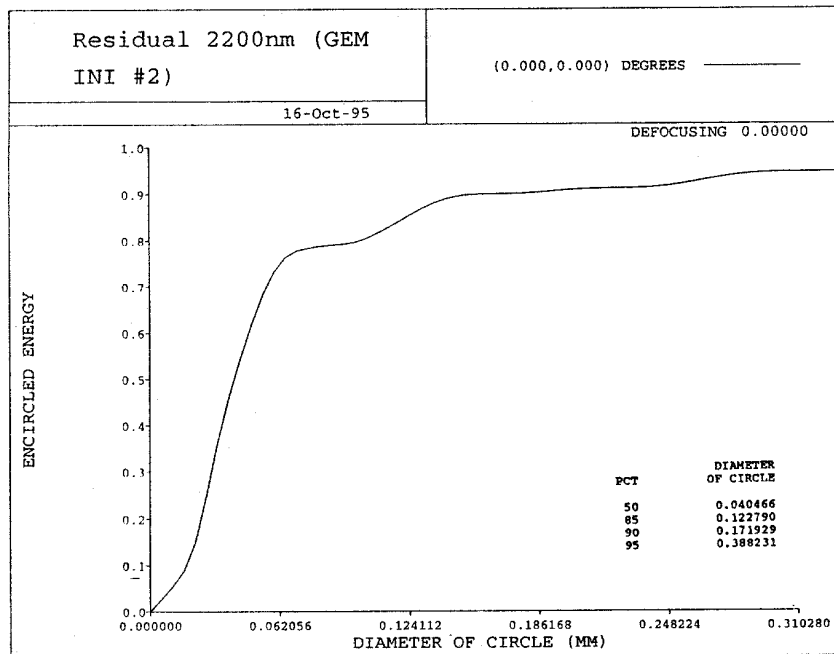


(Encircled energy plot at wl = 2200 nm)

Figure 11. PSF and Encircled energy plots (CASE_1G)

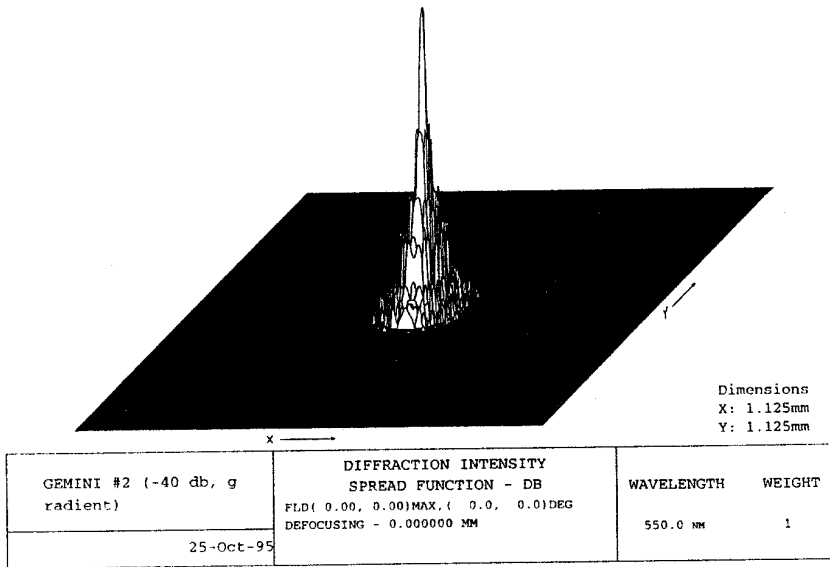


(PSF plot with cutoff = -40 dB at wl = 550 nm)

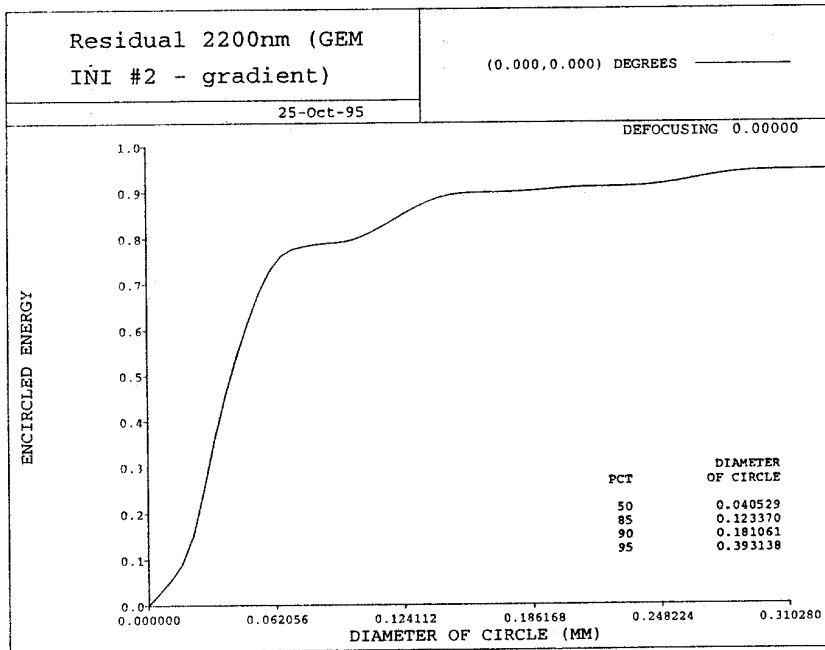


(Encircled energy plot at wl = 2200 nm)

Figure 12. PSF and Encircled energy plots (CASE_2S)



(PSF plot with cutoff = -40 dB at wl = 550 nm)



(Encircled energy plot at wl = 2200 nm)

Figure 13. PSF and Encircled energy plots (CASE_2G)